





Anodic instability of carbon in non-alkaline Zn–air batteries†

Roman R. Kapaev * and Malachi Noked *

Cite this: *Chem. Commun.*, 2023, 59, 9856

Received 21st May 2023,
Accepted 18th July 2023

DOI: 10.1039/d3cc02458j

rsc.li/chemcomm

Although non-alkaline rechargeable Zn–air batteries (RZABs) are promising for energy storage, their chemistry is still underdeveloped and unclear. It was suggested that using Zn(OAc)₂ or Zn(OTf)₂ aqueous solutions as electrolytes enables reversible, corrosion-free charge–discharge processes, but the anodic stability of carbon in these cells has remained poorly studied. We report that CO₂ evolution is manifested during the oxygen evolution reaction in non-alkaline RZABs, which is associated with the corrosion of carbon scaffolds. This corrosion is observed for different electrolyte compositions, such as Zn(OAc)₂, ZnSO₄ and Zn(OTf)₂ solutions of various concentrations. The corrosion rate decreases when the overpotentials during the oxygen evolution reaction are lower. This study underlines the importance of addressing the anodic instability of carbon in non-alkaline RZABs.

Rechargeable Zn–air batteries (RZABs) are a promising technology for energy storage, which can potentially offer high energy density, low cost, and safety.^{1–3} Most of the research in this area pertains to alkaline Zn–air batteries that employ a Zn metal negative electrode (anode), an oxygen-breathing positive electrode (cathode), and a strongly basic electrolyte, such as 6M KOH.^{1,4} However, there are several drawbacks that limit their performance and impede practical applications.⁵ There is uneven vertical growth of Zn and passivation of the Zn anode, which makes the batteries unstable.^{6,7} Continuous corrosion of zinc occurs in alkaline electrolytes, resulting in the loss of active Zn and fast cell degradation.⁷ Consumption of CO₂ from the atmosphere, which is inevitable if ambient air is used, leads to clogging of the cathodes with K₂CO₃.⁸ Finally, a significant problem is the corrosion of carbon that was reported in alkaline RZABs.^{9–12} The oxidation of carbon results in catalytic activity loss and the formation of the same K₂CO₃ that clogs the pores of positive electrodes.

Many of these problems can be circumvented by using non-alkaline electrolytes. Zinc anodes are more stable in near-neutral media, resulting in higher coulombic efficiency and generally smoother plating-stripping behavior.¹³ Additionally, irreversible CO₂ uptake is no longer a critical problem in non-alkaline systems.^{14,15} It could be suggested that corrosive processes should also be suppressed in less aggressive environments of mild electrolytes. However, the anodic stability of carbon in non-alkaline RZABs has not been studied thoroughly. Sun *et al.*¹⁴ reported that no CO₂ evolution was observed with 1 M Zn(OTf)₂ electrolyte, although their cells could be easily overcharged, which indicates the presence of a parasitic oxidation reaction at the positive electrode side. 1 M Zn(OAc)₂ was also reported as a promising electrolyte that might enable stable cycling,¹⁵ but corrosion of carbon was not studied for this system. Here we gain a detailed insight into the anodic stability of carbon in RZABs with various non-alkaline electrolytes using online electrochemical mass spectrometry (OEMS) and complementary techniques.

Initially, aqueous 1 M solutions of Zn(OAc)₂, ZnSO₄ and Zn(OTf)₂ were selected as electrolytes. Acetate- and triflate-based compositions were reported to be promising for RZABs,^{14,15} and the sulfate-based solution is attractive because of low cost and electrochemical stability of the SO₄^{2–} anion. Carbon black (Ketjenblack EC300J) was selected as a model cathode material. The cathode substrate was hydrophobic carbon black (Sigracet 39BB), which is electrochemically inactive in the operational voltage range of the cells.¹⁶ Sealed cells that have reservoirs filled with ambient air¹⁶ were subjected to galvanostatic cycling at 1 mA cm^{–2} with a fixed capacity of 1 mA h cm^{–2}. Details are available in the Experimental section.

As shown in Fig. 1, CO₂ evolution is observed during the OEMS experiments for the cells with all electrolyte compositions. Carbon dioxide evolves only during the charge step, which corresponds to the oxygen evolution reaction (OER) at the positive electrode. At the first cycle, the CO₂ evolution rate is smaller with the triflate-based electrolyte, but it increases during subsequent cycling (Fig. 1c). A similar trend is observed

Department of Chemistry and BINA – BIU Center for Nanotechnology and Advanced Materials, Bar-Ilan University, Ramat-Gan 5290002, Israel.

E-mail: kapaevr@biu.ac.il, malachi.noked@biu.ac.il

† Electronic supplementary information (ESI) available. See DOI: <https://doi.org/10.1039/d3cc02458j>



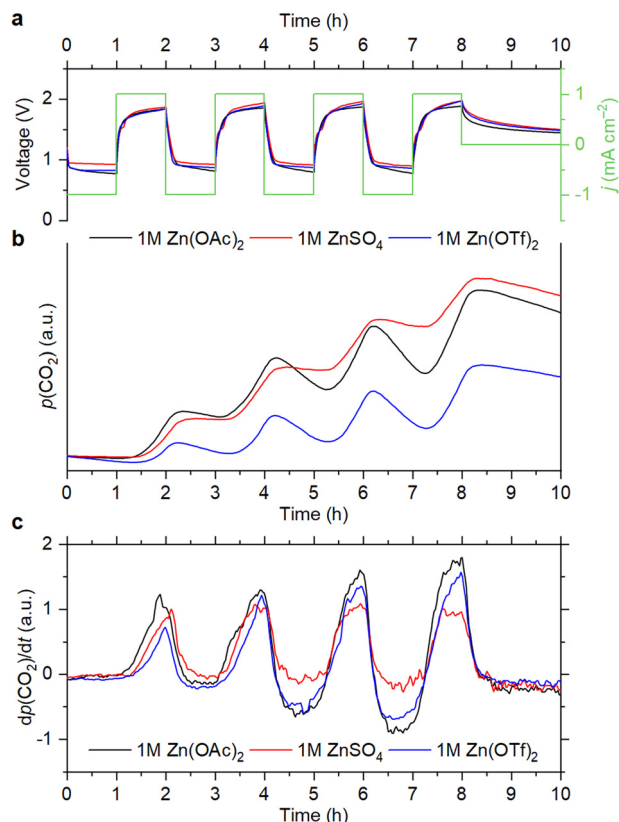


Fig. 1 Cell voltage and current density vs. time (a), evolution of the CO₂ partial pressure (b) and its derivative (c) during the OEMS measurements with 1 M electrolytes.

with the acetate-based electrolyte during the initial cycles. However, the CO₂ evolution rate stabilizes after the first three cycles (Fig. S1a, ESI†).

After four cycles, the cells were left at an open-circuit voltage (OCV). It is seen that the partial pressure of CO₂ slowly decreases during the OCV step, which is because air is continuously evacuated for mass-spectrometry sampling. Decrease of the CO₂ content is also observed during the cell discharge, which corresponds to the oxygen reduction reaction (ORR). However, it becomes faster upon cycling than during the OCV step (Fig. 1b, c and Fig. S1, ESI†). Since electrochemical reduction of CO₂ is completely inhibited when the O₂ concentration is high, it cannot cause a pronounced decrease of the CO₂ level.¹⁷ This indicates that absorption of CO₂ by the electrolytes takes place during the ORR. It should be noted that 4e⁻ O₂ reduction is observed with each of the selected electrolytes (see Section S1, ESI†), which is accompanied by the generation of OH⁻ ions.^{14,15,18} Therefore, it is suggested that absorption of CO₂ is associated with an increase of pH, which was previously reported for non-alkaline RZABs.^{14,18} It is seen that the CO₂ uptake becomes more pronounced upon cycling. With the Zn(OAc)₂ and Zn(OTf)₂ solutions, this effect becomes obvious after two cycles (Fig. 1c); with the ZnSO₄ solution, it becomes evident after four cycles (Fig. S1b, ESI†). Supposedly, pH gradually increases due to the accumulation of discharge products, eventually reaching values that promote

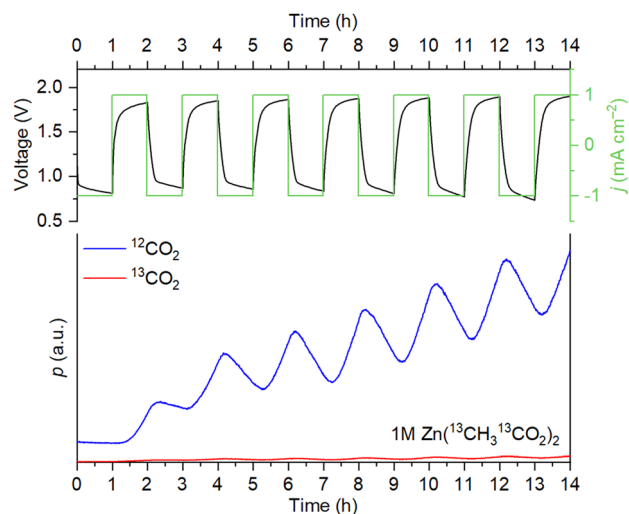


Fig. 2 Cell voltage/current density vs. time and evolution of ¹²CO₂/¹³CO₂ during the OEMS measurements with 1 M Zn(¹³CH₃¹³CO₂)₂ as the electrolyte.

the absorption of carbon dioxide. Further studies of the pH evolution in the cells are required to understand this phenomenon.

For the triflate- and sulfate-based systems, the only source of evolving CO₂ is the corrosion of the carbon scaffold. For Zn(OAc)₂, however, decarboxylation of acetate ions according to the Kolbe reaction is also possible.¹⁹ To determine if acetate oxidation takes place, we monitored ¹²CO₂/¹³CO₂ evolution during cycling with a 1 M solution of labeled zinc acetate, Zn(¹³CH₃¹³CO₂)₂. It is seen in Fig. 2 that the evolution of ¹²CO₂ is mostly observed. The ratio between the ¹³CO₂ and ¹²CO₂ signal intensities does not increase during the OER steps. Therefore, the decomposition of acetate is absent, and CO₂ evolution is associated solely with the corrosion of the carbon electrodes.

To track the evolution of the carbon surface, we compared the C1s X-ray photoelectron spectra (XPS) of the electrodes before and after cycling. The cell with 1 M ZnSO₄ solution was selected as a model system to avoid interference with carbon atoms from the electrolyte. In the corroded electrode, the peak at 286 eV, which corresponds to C–O groups,^{20,21} has an increased relative intensity (Fig. 3a). The estimated content of C–O carbons raises from 11% to 16% at. after ten cycles. Additionally, Raman spectroscopy shows that corrosion leads to a decrease of the D/G and D*/G band ratios (Fig. 3b), which correspond to disordered domains in carbon black.^{22–24} Therefore, the disordered domains are more susceptible to oxidation than graphitic sp² domains, which is in accordance with the literature.^{25–27} In the scanning electron microscopy (SEM) images, hexagonal platelets are observed in the electrode after cycling (Fig. 3c). These particles are attributed to the zinc hydroxysulfate discharge product,¹⁴ which does not decompose completely during the OER because the charge-discharge is only partially reversible.

A popular strategy to improve the stability of batteries at high voltages is to increase the salt concentration in the



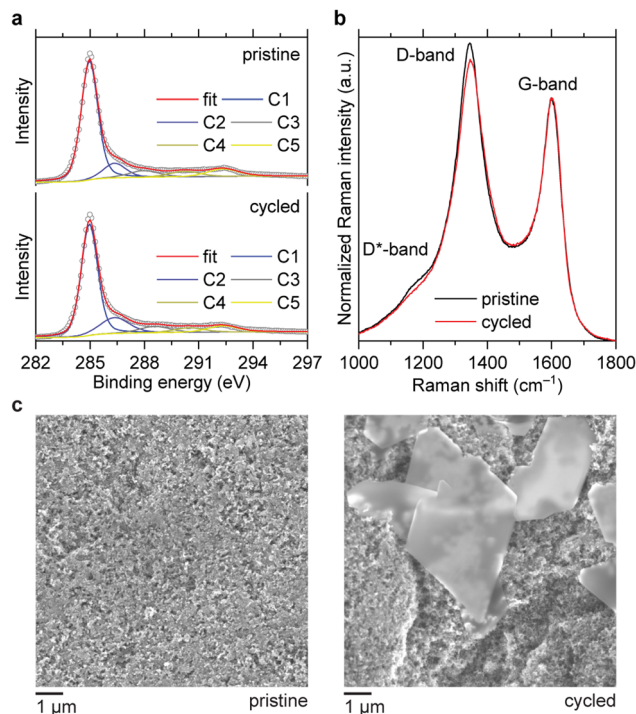


Fig. 3 XPS (a), Raman spectra (b) and SEM images (c) of the carbon electrodes before and after 10 cycles at 1 mA cm⁻² with a fixed capacity of 1 mA h cm⁻². The electrolyte was 1 M ZnSO₄.

electrolytes.²⁸ To see if carbon corrosion can be mitigated using this approach, we performed comparative OEMS experiments with different salt concentrations. The data indicate that using more concentrated electrolytes does not lead to any substantial decrease of the CO₂ evolution rate during the OER (Fig. S2, ESI†). On the other hand, it is seen that CO₂ absorption during the ORR is slightly less pronounced when concentrated Zn(OAc)₂ and Zn(OTf)₂ solutions are used. This is likely associated with the higher buffering capacity of the concentrated electrolytes, which decreases the variation of pH upon cycling.

To see how the corrosion depends on the OER performance of carbons, we compared the CO₂ evolution rates for Ketjen-black EC300J and Ketjenblack EC600JD. These carbons have almost identical particle size, graphitization degree, surface chemistry and wettability properties, but EC600JD has a higher specific surface area (1444 m² g⁻¹ vs. 451 m² g⁻¹), which results in lower OER overpotentials.¹⁶ Despite a more developed surface of EC600JD, which should make it more susceptible to oxidation,²⁹ it is observed that the CO₂ evolution rate for EC600JD is lower than for EC300J (Fig. 4). Therefore, it might be concluded that the carbon corrosion rate might be mitigated by decreasing the OER overpotentials. This is also confirmed by running OEMS at different current rates (0.5 and 1 mA cm⁻²). Applying smaller current results in lower overpotentials, and lower CO₂ evolution rates are observed accordingly (Fig. S3, ESI†).

To summarize, this study shows that oxidation of carbon takes place during the OER in non-alkaline RZABs. Carbon corrosion is observed for Zn(OAc)₂, Zn(OTf)₂ and ZnSO₄-based

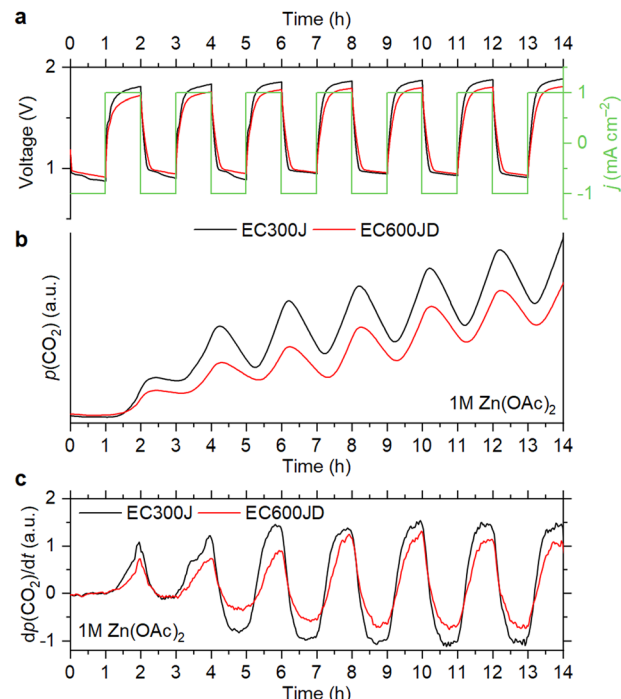


Fig. 4 Cell voltage and current density vs. time (a), evolution of CO₂ partial pressure (b) and its derivative (c) during the OEMS measurements with different types of carbon black. The electrolyte was 1 M Zn(OAc)₂.

electrolytes with various salt concentrations. Additionally, we demonstrate that acetate anions are stable during the OER, and CO₂ absorption occurs during the ORR, presumably because of a pH increase that takes place upon cell discharging. Overall, the results highlight that addressing the anodic instability of positive electrodes is crucial for non-alkaline Zn-air batteries. Suggested ways to suppress the carbon corrosion include enhancement of the OER kinetics and increasing the graphitization degree. Supposedly, the corrosion might also be circumvented by depositing protective coatings at the carbon surfaces.

R. R. K. and M. N. conceived the project. R. R. K. designed and performed the experiments and wrote the manuscript. M. N. edited the manuscript and supervised the project.

This work was financially supported by Nichia Corporation. The authors thank their colleagues from Bar-Ilan University: Michal Ejgenberg for XPS measurements, Amit Ohayon for SEM measurements, and Sri Harsha Akella for the help with OEMS measurements.

Conflicts of interest

There are no conflicts to declare.

References

- 1 K. W. Leong, Y. Wang, M. Ni, W. Pan, S. Luo and D. Y. C. Leung, *Renew. Sustainable Energy Rev.*, 2022, **154**, 111771.
- 2 J. W. Choi and D. Aurbach, *Nat. Rev. Mater.*, 2016, **1**, 16013.
- 3 Q. Liu, L. Wang and H. Fu, *J. Mater. Chem. A*, 2023, **11**, 4400–4427.
- 4 Y. Wei, Y. Shi, Y. Chen, C. Xiao and S. Ding, *J. Mater. Chem. A*, 2021, **9**, 4415–4453.



- 5 D. Deckenbach and J. J. Schneider, *Adv. Mater. Interfaces*, 2023, **10**, 2202494.
- 6 J. Zhang, Q. Zhou, Y. Tang, L. Zhang and Y. Li, *Chem. Sci.*, 2019, **10**, 8924–8929.
- 7 J. Yi, P. Liang, X. Liu, K. Wu, Y. Liu, Y. Wang, Y. Xia and J. Zhang, *Energy Environ. Sci.*, 2018, **11**, 3075–3095.
- 8 S. Zhao, T. Liu, J. Wang, I. Temitope Bello, Y. Zuo, M. Wei, K. Wang, K. K. S. Lau and M. Ni, *Chem. Eng. J.*, 2022, **450**, 138207.
- 9 Y. He, W. Shang, M. Ni, Y. Huang, H. Zhao and P. Tan, *Chem. Eng. J.*, 2022, **427**, 130862.
- 10 T. Wang, M. Kunitomo, T. Mori, M. Yanagisawa, J. Niikura, I. Takahashi, M. Morita, T. Abe and T. Homma, *J. Power Sources*, 2022, **533**, 231237.
- 11 Z. Zhao, W. Yu, W. Shang, Y. He, Y. Ma, Z. Zhang and P. Tan, *J. Power Sources*, 2022, **543**, 231844.
- 12 S. Möller, S. Barwe, J. Masa, D. Wintrich, S. Seisel, H. Baltruschat and W. Schuhmann, *Angew. Chem., Int. Ed.*, 2020, **59**, 1585–1589.
- 13 C. Li, L. Wang, J. Zhang, D. Zhang, J. Du, Y. Yao and G. Hong, *Energy Storage Mater.*, 2022, **44**, 104–135.
- 14 W. Sun, F. Wang, B. Zhang, M. Y. Zhang, V. Kupers, X. Ji, C. Theile, P. Bieker, K. Xu, C. S. Wang and M. Winter, *Science*, 2021, **371**, 46–51.
- 15 W. Sun, V. Küpers, F. Wang, P. Bieker and M. Winter, *Angew. Chem., Int. Ed.*, 2022, **61**, e202207353.
- 16 R. R. Kapaev, A. Ohayon, M. Sonoo, J. Tzadikov, M. Shalom and M. Noked, *Electrochim. Acta*, 2023, **456**, 142462.
- 17 Y. Xu, J. P. Edwards, J. Zhong, C. P. O'Brien, C. M. Gabardo, C. McCallum, J. Li, C.-T. Dinh, E. H. Sargent and D. Sinton, *Energy Environ. Sci.*, 2020, **13**, 554–561.
- 18 S. Clark, A. R. Mainar, E. Iruin, L. C. Colmenares, J. A. Blázquez, J. R. Tolchard, A. Latz and B. Horstmann, *J. Mater. Chem. A*, 2019, **7**, 11387–11399.
- 19 N. Sbei, S. Aslam and N. Ahmed, *React. Chem. Eng.*, 2021, **6**, 1342–1366.
- 20 J. Park, W. Lee, J. Nam, J. T. Han, C.-J. Choi and J. Y. Hwang, *Carbon*, 2022, **189**, 579–585.
- 21 I. Ferrari, A. Motta, R. Zanon, F. A. Scaramuzza, F. Amato, E. A. Dalchiele and A. G. Marrani, *Carbon*, 2023, **203**, 29–38.
- 22 A. Y. Lee, K. Yang, N. D. Anh, C. Park, S. M. Lee, T. G. Lee and M. S. Jeong, *Appl. Surf. Sci.*, 2021, **536**, 147990.
- 23 S. Potgieter-Vermaak, N. Maledi, N. Wagner, J. H. P. Van Heerden, R. Van Grieken and J. H. Potgieter, *J. Raman Spectrosc.*, 2011, **42**, 123–129.
- 24 A. Sadezky, H. Muckenhuber, H. Grothe, R. Niessner and U. Pöschl, *Carbon*, 2005, **43**, 1731–1742.
- 25 L. Dubau, L. Castanheira, F. Maillard, M. Chatenet, O. Lottin, G. Maranzana, J. Dillet, A. Lamibrac, J.-C. Perrin, E. Moukheiber, A. ElKaddouri, G. De Moor, C. Bas, L. Flandin and N. Caqué, *Wiley Interdiscip. Rev.: Energy Environ.*, 2014, **3**, 540–560.
- 26 J. Yang, S. Park, K. Y. Choi, H.-S. Park, Y.-G. Cho, H. Ko and H.-K. Song, *ACS Sustainable Chem. Eng.*, 2018, **6**, 9566–9571.
- 27 Y. Yi, G. Weinberg, M. Prenzel, M. Greiner, S. Heumann, S. Becker and R. Schlögl, *Catal. Today*, 2017, **295**, 32–40.
- 28 Y. Yamada, J. Wang, S. Ko, E. Watanabe and A. Yamada, *Nat. Energy*, 2019, **4**, 269–280.
- 29 S. C. Ball, S. L. Hudson, D. Thompson and B. Theobald, *J. Power Sources*, 2007, **171**, 18–25.

